

## Linear polarization fractions of Fulcher- $\alpha$ fluorescence in electron collisions with H<sub>2</sub>

Liam H. Scarlett<sup>1,\*</sup> Una S. Rehill,<sup>1</sup> Mark C. Zammit<sup>2,3</sup>, Klaus Bartschat<sup>3</sup>, Igor Bray<sup>1</sup>, and Dmitry V. Fursa<sup>1</sup>

<sup>1</sup>Curtin Institute for Computation and Department of Physics, Astronomy and Medical Radiation Sciences,

Curtin University, Perth, Western Australia 6102, Australia

<sup>2</sup>Theoretical Division, Los Alamos National Laboratory, Los Alamos, New Mexico 87545, USA

<sup>3</sup>Department of Physics and Astronomy, Drake University, Des Moines, Iowa 50311, USA



(Received 6 August 2021; accepted 20 September 2021; published 12 October 2021)

We apply the molecular convergent close-coupling method to the calculation of linear polarization fractions for Fulcher-band fluorescence following electron-impact excitation of the H<sub>2</sub>  $d^3\Pi_u$  state. The results exhibit the opposite threshold behavior compared to the only previous calculations [Meneses, Brescansin, Lee, Michelin, Machado, and Csanak, *Phys. Rev. A* **52**, 404 (1995)], but are in agreement with the most recent measurements for the  $Q(1)$ ,  $R(1)$ , and  $Q(3)$  transitions [Maseberg, Bartschat, and Gay, *Phys. Rev. Lett.* **111**, 253201 (2013)].

DOI: [10.1103/PhysRevA.104.L040801](https://doi.org/10.1103/PhysRevA.104.L040801)

Measurements of collisionally induced fluorescence can reveal features of the collision dynamics not probed in standard scattering experiments, and hence provide some of the most sensitive tests of quantum-mechanical scattering theories. With the considerable progress made in computational methods over the past few decades, it is now commonplace to see outstanding agreement between measured and calculated Stokes parameters for scattering on atomic targets. However, in the case of molecular targets, both measurements and calculations of Stokes parameters are rare, and previous studies have not shown satisfactory agreement between theory and experiment.

For low-temperature hydrogen plasmas, the H<sub>2</sub> Fulcher- $\alpha$  ( $d^3\Pi_u \rightarrow a^3\Sigma_g^+$ ) band is of particular interest in optical emission spectroscopy as a diagnostic tool [1], and has therefore attracted much attention from both theorists and experimentalists. The most recent measurements are due to Maseberg *et al.* [2], who measured the linear and circular polarization fractions of Fulcher- $\alpha$  fluorescence following spin-polarized electron collisions with ortho-H<sub>2</sub>. The novel aspect of these results is the behavior of the linear polarization fraction, which reaches negative values at near-threshold energies, in contrast to the only previous calculations [3], which predicted the opposite near-threshold behavior for the  $Q(1)$  transition.

In this Letter, we apply the molecular convergent close-coupling (MCCC) method [4] to the calculation of rovibrationally resolved cross sections for the electron-impact  $X^1\Sigma_g^+ \rightarrow d^3\Pi_u$  transition, and subsequently calculate the linear polarization fractions  $P_1$  for the Fulcher- $\alpha$  fluorescence. The MCCC method has previously been shown to accurately solve the  $e^-$ -H<sub>2</sub> electronic scattering problem in Refs. [5,6]. It has since been extended with the adiabatic-nuclei approximation to produce a comprehensive set of vibrationally resolved electronic excitation cross sections for H<sub>2</sub> and its isotopologues [7,8]. The distinctive feature of the MCCC method

is its capacity to run large-scale, fully quantum-mechanical calculations, which are accurate over the entire range of projectile energies.

The Fulcher- $\alpha$  transitions measured by Maseberg *et al.* [2], which we consider here, are  $Q(1)$ ,  $R(1)$ , and  $Q(3)$ . These notations are defined in Table I. The vibrational level  $v$  is the same in both the  $d^3\Pi_u$  and  $a^3\Sigma_g^+$  states, and the labeling of rotational levels is according to Hund's case (b) [9]. Following the method outlined by Maseberg *et al.* [2], we reevaluated the coefficients and noticed some printing mistakes in their Eqs. (4) and (5). While these do not change the qualitative predictions, the corrected equations for obtaining the linear polarization fraction for these transitions are

$$Q(1) : P_1 = \frac{0.061 A_{20}(1)}{1 + 0.020 A_{20}(1)}, \quad (1)$$

$$R(1) : P_1 = -\frac{0.178 A_{20}(2)}{1 - 0.059 A_{20}(2)}, \quad (2)$$

$$Q(3) : P_1 = \frac{0.321 A_{20}(3)}{1 + 0.107 A_{20}(3)}, \quad (3)$$

where

$$A_{20}(1) = \sqrt{2}(\sigma_1 - \sigma_0)/\sigma(N = 1), \quad (4)$$

$$A_{20}(2) = \sqrt{10/7}(2\sigma_2 - \sigma_1 - \sigma_0)/\sigma(N = 2), \quad (5)$$

$$A_{20}(3) = \sqrt{1/3}(5\sigma_3 - 3\sigma_1 - 2\sigma_0)/\sigma(N = 3). \quad (6)$$

Here,  $\sigma_{m_{N_f}}$  are the cross sections for excitation of the rotational sublevel  $m_{N_f}$  in the rotational level  $N_f$ , and  $\sigma(N_f)$

TABLE I. Definitions of the notation for radiative transitions.

Notation	Transition
$Q(N)$	$d^3\Pi_u^-(v, N) \rightarrow a^3\Sigma_g^+(v, N)$
$R(N)$	$d^3\Pi_u^+(v, N + 1) \rightarrow a^3\Sigma_g^+(v, N)$

\*liam.scarlett@postgrad.curtin.edu.au

is the total cross section for final rotational level  $N_f$ . Both are summed over initial rotational levels and sublevels in the  $X^1\Sigma_g^+$  state assuming a Boltzmann distribution at 300 K to allow comparison with the experimental data of Maseberg *et al.* [2]:

$$\sigma_{m_{N_f}}[n_f v_f N_f \leftarrow n_i v_i] = \sum_{N_i m_{N_i}} p_{N_i} \sigma_{n_f v_f N_f m_{N_f}, n_i v_i N_i m_{N_i}}, \quad (7)$$

$$\sigma(N_f)[n_f v_f \leftarrow n_i v_i] = \sum_{m_{N_f}} \sigma_{m_{N_f}}[n_f v_f N_f \leftarrow n_i v_i], \quad (8)$$

where  $p_{N_i}$  are the Boltzmann weights,  $v_f$  is the vibrational level in the electronic state  $n_f$  ( $d^3\Pi_u$ ), and  $v_i$  is the vibrational level in the electronic state  $n_i$  ( $X^1\Sigma_g^+$ ). Note that here  $v_f$  corresponds to  $v$  in Table I.

In Hund's case (b) [9], the spin-averaged integral rovibronic excitation cross section resolved in rotational sublevels is

$$\begin{aligned} \sigma_{n_f v_f N_f m_{N_f}, n_i v_i N_i m_{N_i}} &= \frac{q_f}{q_i} \frac{1}{4\pi} \sum_{\mathcal{S}} \frac{2\mathcal{S}+1}{2(2s_i+1)} \sum_{\mathcal{J} \mathcal{J}'} \sum_{L_f} \sum_{L_i L_i'} \sqrt{(2L_i+1)(2L_i'+1)} \\ &\times F_{n_f v_f N_f L_f, n_i v_i N_i L_i}^{\mathcal{J} \mathcal{S}} F_{n_f v_f N_f L_f, n_i v_i N_i L_i'}^{\mathcal{J}' \mathcal{S}'} \\ &\times C_{L_i 0, N_i m_{N_i}}^{\mathcal{J} m_{N_i}} C_{L_i' 0, N_i m_{N_i}}^{\mathcal{J}' m_{N_i}} C_{L_f m_{L_f}, N_f m_{N_f}}^{\mathcal{J} m_{N_i}} C_{L_f m_{L_f}, N_f m_{N_f}}^{\mathcal{J}' m_{N_i}}, \end{aligned} \quad (9)$$

where  $q$  is the projectile linear momentum,  $C$  are the standard Clebsch-Gordan coefficients,  $L$  is the projectile partial-wave orbital angular momentum,  $s_i$  is the initial target electronic spin,  $\mathcal{S}$  is the total (projectile plus target) spin,  $\mathcal{J}$  is the total angular momentum excluding spin, and  $F^{\mathcal{J} \mathcal{S}}$  are the laboratory-frame partial-wave scattering amplitudes. For  $\Sigma \rightarrow \Pi$  electronic transitions,  $F^{\mathcal{J} \mathcal{S}}$  has the following form:

$$\begin{aligned} F_{n_f v_f N_f L_f, n_i v_i N_i L_i}^{\mathcal{J} \mathcal{S}} &= \frac{1}{2(2\mathcal{J}+1)} \sqrt{(2N_f+1)(2N_i+1)} \sum_{\Lambda_{L_f} \Lambda_{L_i}} C_{L_f \Lambda_{L_f}, N_f}^{\mathcal{J} \Lambda_{L_i}} \\ &\times [C_{L_f \Lambda_{L_f}, N_f \Lambda_f}^{\mathcal{J} \Lambda_e} F_{n_f(\Lambda_f) v_f L_f \Lambda_{L_f}, n_i v_i L_i \Lambda_{L_i}}^{\mathcal{S}} \\ &+ (-1)^{N_f} C_{L_f \Lambda_{L_f}, N_f -\Lambda_f}^{\mathcal{J} \Lambda_e} F_{n_f(-\Lambda_f) v_f L_f \Lambda_{L_f}, n_i v_i L_i \Lambda_{L_i}}^{\mathcal{S}}]. \end{aligned} \quad (10)$$

Here  $\Lambda_L$  are the body-frame projections of the projectile angular momenta,  $\Lambda_f$  is the body-frame projection of the electronic-state orbital angular momentum, and  $F^{\mathcal{S}}$  are the body-frame partial-wave vibronic scattering amplitudes obtained from adiabatic-nuclei MCCC calculations [7]. In this Letter we consider scattering on ortho-H<sub>2</sub> ( $X^1\Sigma_g^+$  state, nuclear spin  $I=1$ ), which has only odd  $N$  in the  $X^1\Sigma_g^+$  state. Assuming the nuclear spin is unchanged during the collision, the restriction of  $I=1$  allows us to associate odd  $N_f$  in the  $d^3\Pi_u$  state with the  $d^3\Pi_u^-$  branch and even  $N_f$  with the  $d^3\Pi_u^+$  branch.

Figure 1 exhibits the MCCC  $P_1$  fractions for the  $Q(1)$ ,  $R(1)$ , and  $Q(3)$  branches. We have performed calculations for excitation of the  $v_f = 0$  and 2 vibrational levels in the  $d^3\Pi_u$  state, finding essentially no difference between the two for the  $Q(1)$  and  $R(1)$  transitions, and only a small difference at low energies for the  $Q(3)$  transition. Since the measurements of Maseberg *et al.* [2] include only  $v_f = 2$  for  $R(1)$  and  $Q(3)$ ,

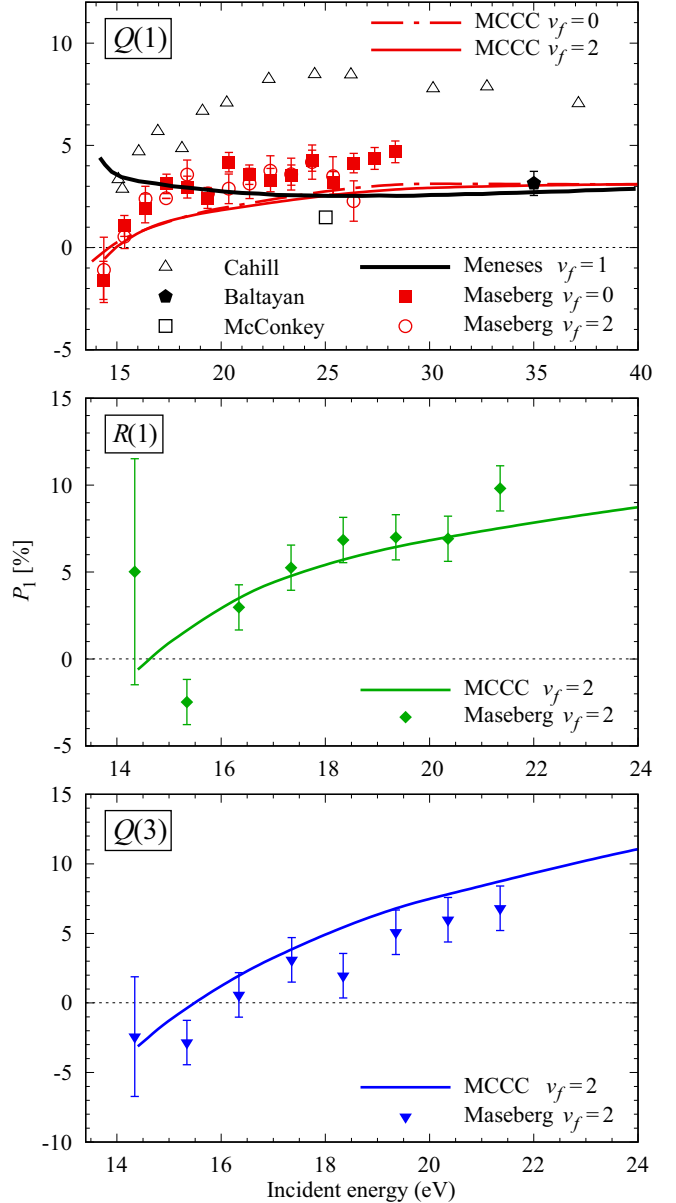


FIG. 1. Linear polarization fraction for the  $Q(1)$ ,  $R(1)$ , and  $Q(3)$  branches in the Fulcher- $\alpha$  band, following electron collisions with ortho-H<sub>2</sub> ( $X^1\Sigma_g^+$ ). Comparisons are made with the measurements of Maseberg *et al.* [2], McConkey *et al.* [10], Baltayan and Nedelec [11], and Cahill *et al.* [12], and the calculations of Meneses *et al.* [3].

we do not present our  $v_f = 0$  results for these transitions for clarity. It is worth noting that the  $d^3\Pi_u$  vibrational levels considered here are not affected by predissociation into the  $a^3\Sigma_g^+$  continuum [13]. The MCCC results reproduce the near-threshold behavior seen in the  $Q(1)$  measurements of Maseberg *et al.* [2], in contrast to the calculations of Meneses *et al.* [3] that predicted the opposite threshold behavior. Quantitatively, the MCCC results are somewhat lower than the measurements of Maseberg *et al.* [2] above 16 eV, with the exception of one point at 26.5 eV, where the measured  $P_1$  fraction for  $v_f = 2$  drops slightly below the MCCC line. At higher energies, the present results appear to converge to the distorted-wave results, and are in agreement with the single

data point of Baltayan and Nedelev [11] at 35 eV. The incorrect near-threshold energy dependence predicted by Meneses *et al.* [3] is likely due to the application of a high-energy approximation (distorted wave) at low incident energies, where it is not accurate. Although the distorted-wave calculations were performed with  $v_f = 1$  only, we have confirmed that the MCCC results for the  $Q(1)$  transition with  $v_f = 1$  are similar to those for  $v_f = 0$  and 2, ensuring that the comparison between the two theoretical methods is valid. For the  $R(1)$  and  $Q(3)$  branches, no previous calculations have been attempted, and measurements have only been reported by Maseberg *et al.* [2]. The agreement between the present results and the measurements for  $R(1)$  is better than for the  $Q(1)$  branch, with the MCCC lines passing through the majority of the experimental data points. There is also satisfactory agreement for the  $Q(3)$  branch, although there appears to be a systematic shift in the calculated values towards the upper limit of the error bars for most experimental points. The reason for this, and for the opposite trend in the  $Q(1)$  results, is not clear at this time.

The good agreement between the MCCC calculations and the most recent measurements [2] of the Fulcher- $\alpha$   $P_1$  fractions is satisfying for three reasons. First, it is a verification of the threshold behavior observed in the experiment, which is unique to molecular targets due to the more complex threshold dynamics than that seen in atomic targets. Second, it is a demonstration that the MCCC method is capable of satisfying one of the most sensitive tests of a quantum-mechanical

scattering theory. Cross-section measurements for this scattering system are rare, and for many transitions the only argument for the accuracy of the MCCC calculations has been the demonstration of convergence [6]. For the  $X^1\Sigma_g^+ \rightarrow d^3\Pi_u$  transition, they have now also been validated by experiment. Finally, information about the Stokes parameters is vital in plasma polarization spectroscopy [14], and the present Letter demonstrates that the MCCC method is capable of providing the necessary data for this diagnostic tool. To this end, we welcome any data requests for additional parameters, transitions, or wider energy ranges than what has been presented here.

This work was supported by the AFOSR and the Australian Research Council. High-performance computing resources were provided by the Pawsey Supercomputing Centre with funding from the Australian Government and Government of Western Australia, and the Texas Advanced Computing Center at The University of Texas at Austin. L.H.S. acknowledges the contribution of an Australian Government Research Training Program Scholarship, and the support of the Forrest Research Foundation. M.C.Z. would like to specifically acknowledge the support of the LANL Laboratory Directed Research and Development program Project No. 20200356ER. LANL is operated by Triad National Security, LLC, for the National Nuclear Security Administration of the U.S. Department of Energy under Contract No. 89233218NCA000001. K.B. acknowledges support from NSF Grants No. PHY-1803844 and No. PHY-2110023.

---

- [1] S. Briefi and U. Fantz, *Plasma Sources Sci. Technol.* **29**, 125019 (2020).
- [2] J. W. Maseberg, K. Bartschat, and T. J. Gay, *Phys. Rev. Lett.* **111**, 253201 (2013).
- [3] G. D. Meneses, L. M. Brescansin, M. T. Lee, S. E. Michelin, L. E. Machado, and G. Csanak, *Phys. Rev. A* **52**, 404 (1995).
- [4] M. C. Zammit, D. V. Fursa, J. S. Savage, and I. Bray, *J. Phys. B* **50**, 123001 (2017).
- [5] M. C. Zammit, J. S. Savage, D. V. Fursa, and I. Bray, *Phys. Rev. Lett.* **116**, 233201 (2016).
- [6] M. C. Zammit, J. S. Savage, D. V. Fursa, and I. Bray, *Phys. Rev. A* **95**, 022708 (2017).
- [7] L. H. Scarlett, D. V. Fursa, M. C. Zammit, I. Bray, Yu. Ralchenko, and K. D. Davie, *At. Data Nucl. Data Tables* **137**, 101361 (2021).
- [8] L. H. Scarlett, D. V. Fursa, M. C. Zammit, I. Bray, and Yu. Ralchenko, *At. Data Nucl. Data Tables* **139**, 101403 (2021).
- [9] J. Brown and A. Carrington, *Rotational Spectroscopy of Diatomic Molecules* (Cambridge University, Cambridge, England, 2003), Chap. 6, pp. 177–301.
- [10] J. W. McConkey, S. Trajmar, J. C. Nickel, and G. Csanak, *J. Phys. B* **19**, 2377 (1986).
- [11] P. Baltayan and O. Nedelev, *J. Phys. (France)* **36**, 125 (1975).
- [12] P. Cahill, R. Schwartz, and A. N. Jette, *Phys. Rev. Lett.* **19**, 283 (1967).
- [13] D. Yamasaki, S. Kado, B. Xiao, Y. Iida, S. Kajita, and S. Tanaka, *J. Phys. Soc. Jpn.* **75**, 044501 (2006).
- [14] *Plasma Polarization Spectroscopy*, edited by T. Fujimoto and A. Iwamae (Springer, New York, 2008), Chap. 1, pp. 1–12.